TÜBİTAK

Turkish Journal of Chemistry

http://journals.tubitak.gov.tr/chem/

Research Article

Turk J Chem
(2019) 43: 50 – 62
© TÜBİTAK
doi:10.3906/kim-1804-20

An evaluation of the adsorption dynamics of phosphate ions onto Fe(II)-montmorillonites

Dawei QIN[1,*], **Shuhua CHANG**[1], **Min QIAO**[2], **Xiaotong YUAN**[1], **Wei LIU**[2], **Gang LIU**[2]
[1]Qilu University of Technology (Shandong Academy of Sciences), Jinan, Shandong, P.R. China
[2]Shandong Bureau of China Metallurgical Geology Bureau Test Center, Jinan, Shandong, P.R. China

Received: 11.04.2018 • **Accepted/Published Online:** 18.09.2018 • **Final Version:** 05.02.2019

Abstract: Fe(II)-montmorillonites (Fe(II)-MMTs) were prepared by mixing solutions of Fe(II) and montmorillonite at pH 3.5. Two different Fe(II)-MMTs were prepared and the ferrous iron contents were 40 mg/L and 80 mg/L. All samples were characterized by XRD, FT-IR, TGA, DSC, and nitrogen adsorption. By nitrogen adsorption, the pore size can be obtained in the pore diameter curve with average pore widths of 6.67 nm, 9.96 nm, and 17.07 nm, respectively. The removal rate of phosphate increased rapidly during the first 40 min, in which Fe(II)-MMT (1) and Fe(II)-MMT (2) were stronger adsorption systems than MMT. The maximum adsorption was 48.38 mg/g at pH 2.0. The kinetics of phosphate adsorption were better described using pseudo-second-order models (R^2: 0.997, 0.999, 1.000) than pseudo-first-order (R^2: 0.933, 0.900, 0.760). R^2 is the determinable statistic coefficient that measures the goodness of fit. If the R^2 value is closer to one, the fitting degree of the regression line is better. By the thermodynamic analyses, we obtained the $\Delta G°$and $\Delta H°$of samples at 298 °C, 303 °C, and 310 °C. The adsorption isotherms also better fitted a Langmuir model in which the process was nonspontaneous and exothermic.

Key words: Fe(II)-montmorillonite, phosphate adsorption, kinetics, hyperphosphatemia

1. Introduction

Montmorillonite (MMT) is a layered silicate mineral that is monoclinic with two layers of a silicon oxygen tetrahedron sandwiching an alumina octahedron that has high ion-exchange capacity.[1] In light of its excellent interlayer cation-exchange capacity (CEC), Fe(II)-MMT was prepared by modification of MMT to specifically target phosphate. Phosphate generally plays an important role in RNA, DNA, and cell metabolism.[2] In addition, excess phosphate can lead to hyperphosphatemia, a common complication arising from chronic kidney disease. Although dialysis treatment is available, a large number of studies and clinical trials have confirmed that hemodialysis does not provide sufficient treatment for hyperphosphatemia: about 80% of dialysis patients still suffer from hyperphosphatemia, resulting in increased mortality.[3–5]

Phosphate adsorption studies have been reported for a number of targets including the environmental and long-term surface properties and stability.[6–8] Fe(III)-MMTS are most commonly obtained and play an important role in organic synthesis. However, no study was found for phosphate adsorption using Fe(II)-MMTs.[9,10]

Two types of Fe(II)-MMTs were prepared. In comparison, three types of samples (MMT, Fe(II)-MMT

*Correspondence: daweiqin109@163.com

(1), and Fe(II)-MMT (2)) were characterized by XRD, FT-IR, TGA, DSC, and nitrogen adsorption.[11–14] The results showed that ferrous ions were adsorbed on the MMT surface or in the interlayer.[15–17] The adsorption experiments of phosphate were carried out at pH 2.0, 7.6, and 8.4 with 0.9% (by wt.%) NaCl. The adsorption quantities of Fe(II)-MMT (1) and Fe(II)-MMT (2) were higher than that of MMT. Two commonly used kinetic models simulated the experimental data: the pseudo-first-order and the pseudo-second-order models.[18–20] Description of the experimental data indicated that the pseudo-second-order model was more suitable.[21–23] Adsorption performance of the modified montmorillonite was better than that of pure montmorillonite.[24–27]

Fe(II)-MMT was prepared by modification of montmorillonite to specifically target phosphate. We can introduce a new method to reduce the concentration of phosphate in RNA, DNA, and cell metabolism. Iron bonds with phosphate forms of insoluble substances that are excreted, while dissociated montmorillonite is not absorbed and thus can be tuned to achieve a therapeutic aim for high phosphorus. Consequently, more dialysis patients will be protected from pain.

2. Results and discussion

2.1. Chemical compositional analysis

The chemical compositions of montmorillonites were determined by X-ray fluorescence spectroscopy. The results are shown in Table 1.

Table 1. The chemical compositions of montmorillonites.

Ions	Si^{4+}	Al^{3+}	Fe^{3+}	Mg^{2+}	Ca^{2+}	K^{1+}	Ti^{4+}	Fe^{2+}	Na^{1+}
Percentage	60.18%	15.79%	5.38%	5.20%	2.32%	0.52%	0.35%	0.12%	0.1%

In addition, there was 2.63% H_2O and a loss on ignition of 7.41% in the montmorillonites. When the adsorption finished, we analyzed the difference between the structures of Fe(II)-MMT and Fe(II)-MMT-P. The results are shown in Figure 1.

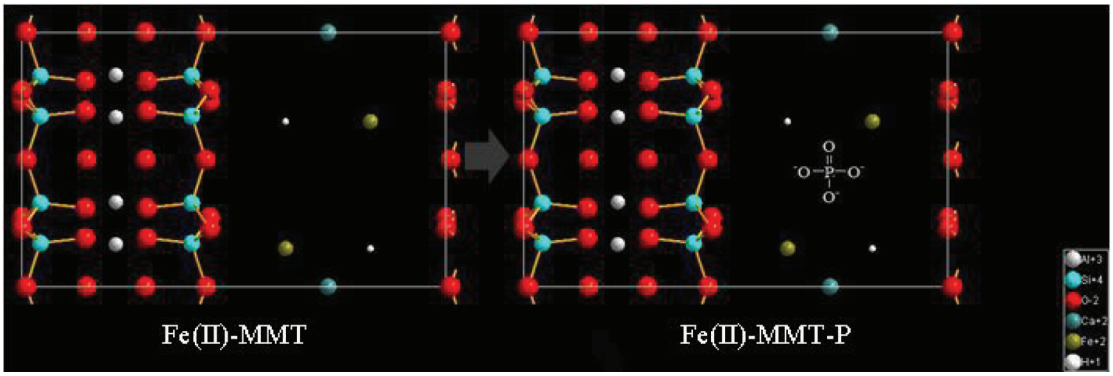

Figure 1. The structures of Fe(II)-MMT and Fe(II)-MMT-P

Types of samples were as follows: (1) raw montmorillonite; (2) montmorillonite with pH 1.0; (3) montmorillonite adsorption of ferrous ion, pH 2.0; and (4) montmorillonite adsorption of ferrous ion, pH 3.5. Then we added six kinds of ions to four different samples. We analyzed the samples with an ICP-5000 spectrometer. The results are shown in Figure 2.

It can clearly be seen that the contents show little change in Figures 2a–2d, while there are much larger changes in Figures 2e and 2f. The intensity of Fe was larger after adsorption, proving that Fe existed in the interlayer or surface of the montmorillonite.

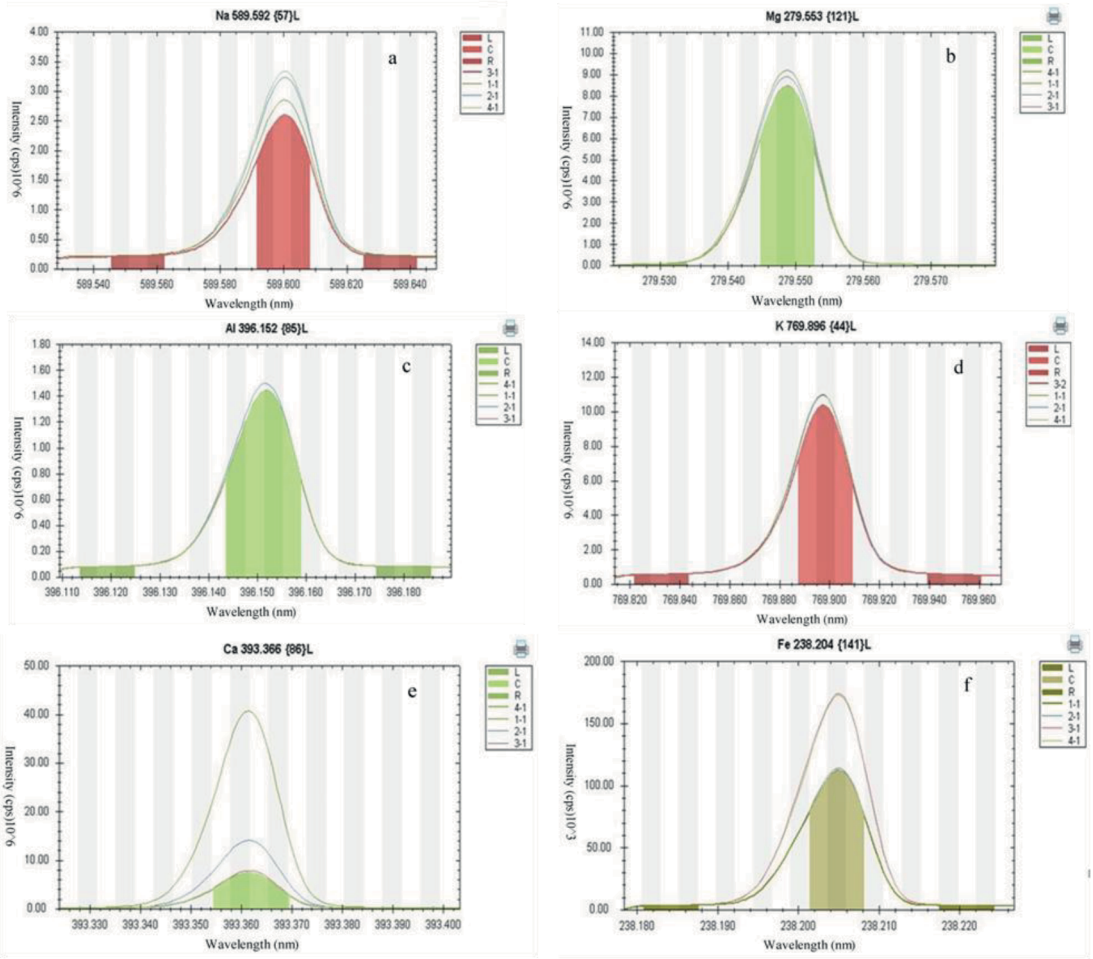

Figure 2. Test results of ICP-5000 spectrometry for samples (six kinds of ions are respectively a: Na, b: Mg, c: Al, d: K, e: Ca, and f: Fe).

2.2. Material characterization

2.2.1. X-ray diffraction analysis

The XRD patterns are shown in Figure 3. The d_{001} basal spacing of the three samples is 15.13 Å, 13.19 Å, and 13.93 Å, which depends on the charge, size, and hydration behavior of the ion located in the interlayer of phyllosilicate layers. The ionic radius of Fe^{2+} is 76 pm, smaller than Na^{+} (102 pm), which can explain the decrease of the basal spacing in principle. The XRD patterns of Fe(II)-MMT (1) are very similar to that of Fe(II)-MMT (2), but the 001 reflection is less intense compared to MMT, proving that a portion of Fe(II) is present in the interlayer space. In addition, the basal spacing of Fe(II)-MMT (2) is slightly larger than that of Fe(II)-MMT (1), suggesting that Fe(II) is present in the interlayer space at a high concentration.

2.2.2. FT-IR analysis

Figure 4 shows the FT-IR spectra (500–4000 cm^{-1}) of three samples. The adsorption bands at 3200–3800 cm^{-1} and 1600–1700 cm^{-1} may be due to OH groups' stretching vibrations The absorption bands at 3431 cm^{-1} and 3628 cm^{-1} were assigned to stretching vibrations of H-O-H and OH groups, respectively. The absorption band at 1641 cm^{-1} is assigned to adsorbed water molecules. The strong absorption peak at 1036 cm^{-1} is the uniquely characteristic stretching vibration of Si-O and Si-O-Si in the mineral layer lattice. The band at 914 cm^{-1} is due to the bending modes of the hydroxyl groups in Al_2OH. The stretching vibrations band at 518 cm^{-1} is sensitive to the presence of Al in the octahedral layer, which suggests that the octahedral Al cations are retained. Thus, the original structure of the montmorillonite was not fully destroyed, in agreement with the XRD results.

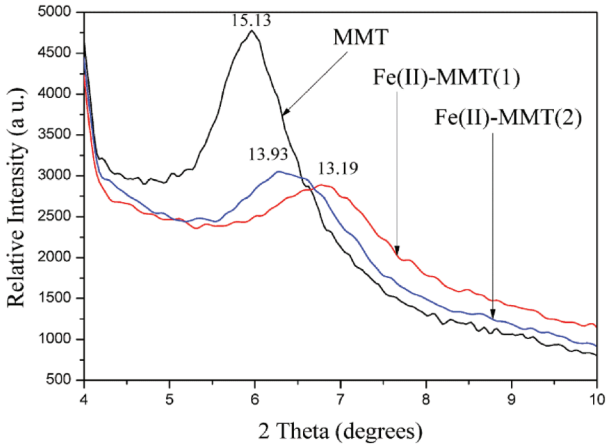

Figure 3. XRD patterns of MMT, Fe(II)-MMT (1), and Fe(II)-MMT (2).

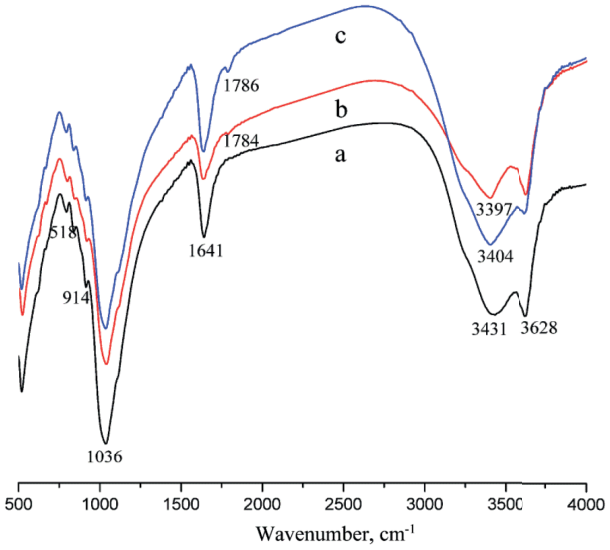

Figure 4. FT-IR patterns of three samples (a: MMT, b: Fe(II)-MMT (1), and c: Fe(II)-MMT (2)).

The FT-IR spectra of the three samples are approximately the same. However, new stretching vibrations modes at 1784 cm^{-1} and 1786 cm^{-1} are observed in Fe(II)-MMT (1) and Fe(II)-MMT (2), respectively, which may arise from iron species internal or external to MMT. The differences among the three samples may be due to different charges, ionic radii, and high ionic concentrations in the interlayer.

2.2.3. Thermogravimetric analysis and differential scanning calorimetry

The thermal behavior of the three samples was studied by TGA and DSC in nitrogen up to 900 °C. As shown in Figure 5, the TGA thermogram of three samples showed a large loss in mass while heating to 120 °C; more specifically, the weight losses were 13.72%, 7.78%, and 8.83%, characterized by the loss of interlayer water and adsorbed water. The endothermic peaks at 80 °C and 120 °C in the DSC curve also confirm this contribution. Upon heating to 630 °C, the weight losses were 0.97%, 1.54%, and 2.08%, respectively, due to the structure of water hydrogen-bonded in the interlayer of MMT. After 630 °C, the montmorillonite interlayer structure began to collapse. The weight decrease and endothermic peak can be observed from the TGA and DSC curves. In Figure 5, it is shown that the thermal stability increased after adsorption of ferrous ions, which proved that modified montmorillonite had increased thermal stability.

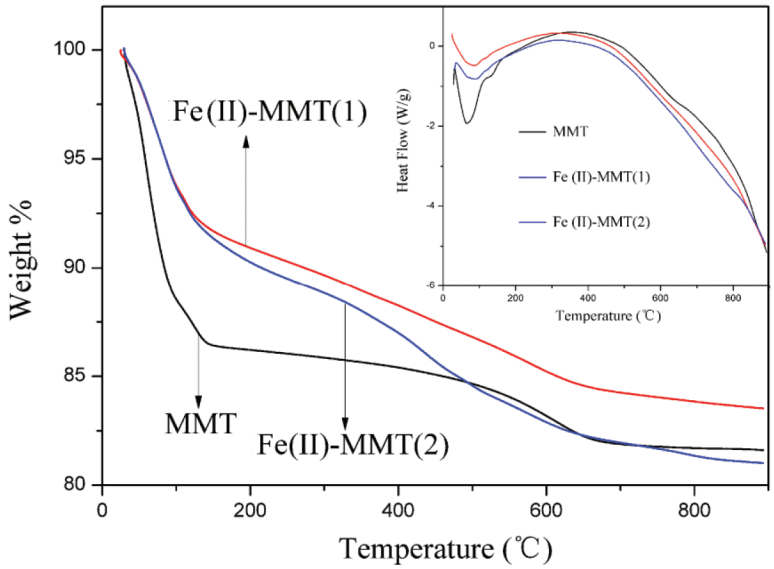

Figure 5. TGA and DSC curves of montmorillonites and montmorillonites with different adsorbed concentrations of ferrous ions.

2.2.4. BET surface areas and N_2 adsorption-desorption isotherms

Table 2 summarizes the textural characteristics of the MMT, Fe(II)-MMT (1), and Fe(II)-MMT (2) samples. The specific surface areas of the three samples were calculated by the multiple-point Brunauer–Emmett–Teller (BET) method, whereas the pore size distribution was calculated using the Barrett–Joyner–Halenda method. The t-plot method was used to compute the microporous and external surface areas. The single-point surface area at P/P_0 was evaluated from nitrogen uptake and was 0.23, 0.99, and 0.99, respectively. MMT presents a surface area of 71.90 m^2/g, while the MMT surface area significantly decreases after adsorption of ferrous ions. The values for the BET surface areas of Fe(II)-MMT (1) and Fe(II)-MMT (2) are 33.69 m^2/g and 6.35 m^2/g, respectively. The reason why the BET surface area of Fe(II)-MMT (1) is far greater than that of Fe(II)-MMT (2) is because of different ionic radii, consistent with XRD analysis. The N_2 adsorption-desorption isotherms of the three samples belong to type IV with H3 hysteresis loops in IUPAC classification. As reported in Figure 6, the adsorption slowly increased at low pressure, which reflects N_2 molecular adsorption on the inner surface of the mesoporous single-to-multilayer system. There is a jump in adsorption quantity at p/p_0 0.43–0.46 that reflects the size of the sample size and suggests a mesoporous system. Adsorption increased at a higher pressure, which reflects the accumulation of macroporous or mesoporous domains. The pore size can also be seen in the pore diameter curve, whose average pore widths are 6.67 nm, 9.96 nm, and 17.07 nm, respectively. This suggests that ferrous ions increased the pore size of the samples as they ingressed into the montmorillonite layers.

2.3. Phosphate sorption kinetics

The adsorption of phosphate by MMT, Fe(II)-MMT (1), and Fe(II)-MMT (2) as a function of time at initial phosphate concentration of 40 mg/g is displayed in Figure 7 (adsorption at pH 2.0). Phosphate can diffuse into the inner surface of pores through mesopores and micropores. The phosphate adsorption of Fe(II)-MMT (1) and Fe(II)-MMT (2) increased rapidly within 40 min and gradually increased for MMT. The adsorption quantities of Fe(II)-MMT (1) and Fe(II)-MMT (2) are greater than that of MMT during the whole adsorption.

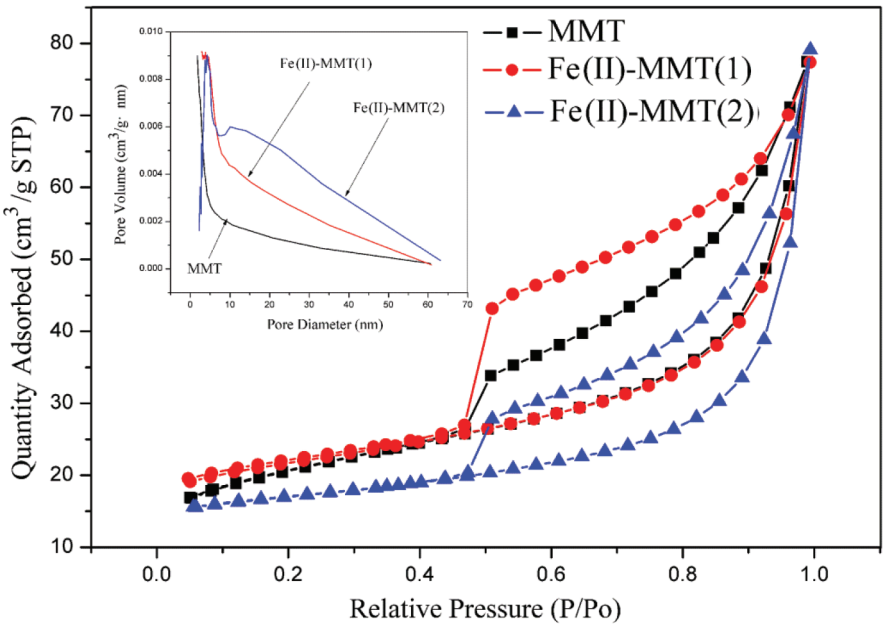

Figure 6. N_2 adsorption-desorption isotherms and pore size curves of MMT, Fe(II)-MMT (1), and Fe(II)-MMT (2).

Table 2. Textural characteristic of the MMT, Fe(II)-MMT (1), and Fe(II)-MMT (2) samples.

Samples	BET surface area (m^2/g)	t-Plot external surface area (m^2/g)	t-Plot micropore volume (cm^3/g)	Adsorption average pore width (nm)
MMT	71.90	48.95	0.0104	6.67
Fe(II)-MMT (1)	33.69	27.90	0.0025	9.96
Fe(II)-MMT (2)	6.35	5.48	0.0004	17.07

The main reason is that silicate minerals such as montmorillonites show a lower affinity for phosphate than does the modified clay. It is well known that the surface of montmorillonite possesses negative charges that logically repel adsorption of (–3 valency) phosphate. The adsorption of phosphate is only at the clay edges. However, after adsorption of ferrous ions, the adsorption quantity jumped significantly. Mineral clays coated with Fe oxides are better phosphate adsorbents than pure montmorillonites due to the electrostatic shielding effect of the oxides. Thus, phosphate adsorption within Fe(II)-MMT (1) and Fe(II)-MMT (2) is due to ferrous ions.

To investigate the process in the adsorption of phosphate, Fe(II)-MMT (1) and Fe(II)-MMT (2), two of the most widely applied kinetic models, pseudo-first-order kinetic Eq. (1)[28,29] and pseudo-second-order kinetic Eq. (2),[30–33] were used to fit the experimental data:

$$\ln(q_e - q_t) = \ln q_e - k_1 t \tag{1}$$

$$t/q_t = 1/(k_2 q_e^2) + t/q_e \tag{2}$$

Here, q_e (mg/g) is the adsorption capacity at adsorption equilibrium, q_t (mg/g) is the adsorption at time t (min), and k_1 (mg/min) and k_2 (mg/min) are the kinetic rate constants for the pseudo-first-order and the pseudo-second-order models,[34–36] respectively.

Table 3 summarizes the equilibrium adsorption quantity, rate constants, and correlation of the two kinetic models obtained from the slope and intercept of each model.

The R^2 (pH 2.0) values from the pseudo-second-order model fitting of MMT, Fe(II)-MMT (1), and Fe(II)-MMT (2) were 0.997, 0.999, and 1.000, respectively, while R^2 are 0.933, 0.900, and 0.760 for the pseudo-first-order model fitting. It was also the same at pH 7.6 and 8.4. Thus, the process of adsorption is better fitted to a pseudo-second-order model while the kinetic parameters demonstrated that the effect of adsorption at pH 2.0 was better than at pH 7.6 and 8.4. The maximum adsorption was 48.38 mg/g at pH 2.0.

2.4. Adsorption isotherms

Figure 8 presents the adsorption isotherms of phosphate on MMT, Fe(II)-MMT (1), and Fe(II)-MMT (2) at 298 K (303 K and 310 K are not shown). The adsorption isotherms were obtained by using initial concentrations ranging from 10 to 120 mg/L.

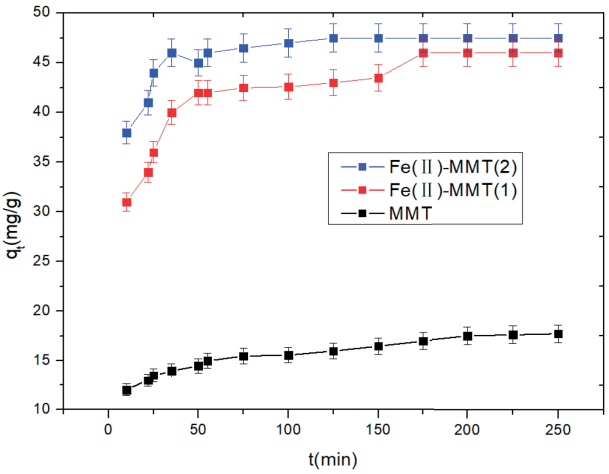

Figure 7. Effect of time on the adsorption of MMT and Fe(II)-MMT (1) and Fe(II)-MMT (2) for phosphate (adsorption conditions: initial condition 40 mg/L, pH 2.0, temperature 310 K).

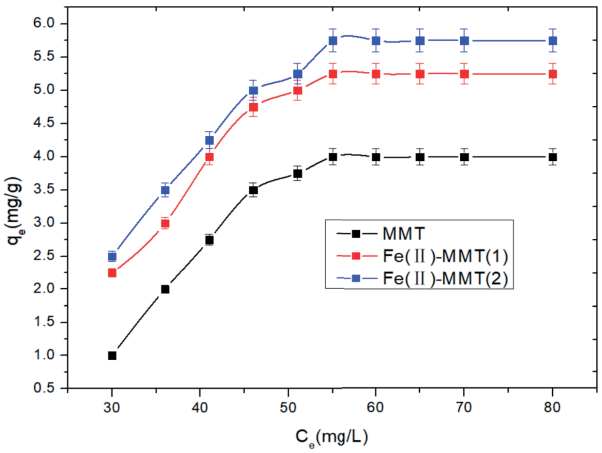

Figure 8. Adsorption isotherm of MMT, Fe(II)-MMT (1), and Fe(II)-MMT (2) for adsorption of phosphate (adsorption conditions: initial condition 40 mg/L, pH 2.0, and temperature 298 K).

Figure 9 provides Langmuir and Freundlich fitted adsorption isotherms of phosphate on MMT, Fe(II)-MMT (1), and Fe(II)-MMT (2) at 298 K (plots at 303 K and 310 K are not shown), respectively. Langmuir isotherm Eq. (3) is given by:

$$1/q_e = 1/q_m + 1/(q_m K_L C_e) \tag{3}$$

Here, q_e (mg/g) is the amount adsorbed at equilibrium, q_m (mg/g) is the maximum monolayer adsorption capacity, K_L (L/mg) is related to the free energy of adsorption, and C_e (mg/L) is the equilibrium concentration of phosphate in solution, respectively. Plots of $1/q_e$ versus $1/C_e$ values can be used to determine q_m and b.

Freundlich isotherm Eq. (4) is an empirical equation given by:

$$\ln q_e = \ln K_F + (1/n) ln C_e \tag{4}$$

Here, q_e (mg/g) is the amount adsorbed at equilibrium; K_F [mg/g (L/mg) 1/n], n is the empirical parameter related to the adsorption capacity and intensity adsorption; and C_e (mg/L) is the equilibrium concentration of the phosphate in solution. The linear plot of ln q_e versus ln C_e can be obtained with K_F and n.

Table 3. Kinetic parameters for phosphate adsorption on three samples.

Samples		Pseudo-first-order model			Pseudo-second-order model		
		k_1 (g^{-1} min^{-1})	R^2	q_{e1} (mg g^{-1})	k_2 (g^{-1} min^{-1})	R^2	q_{e2} (mg g^{-1})
MMT	pH 2.0 pH 7.6 pH 8.4	7×10^{-4}	0.9333	36.86	3.9×10^{-3}	0.9972	19.14
		6×10^{-4}	0.9277	35.12	3.7×10^{-3}	0.9958	18.78
		5×10^{-4}	0.9189	34.56	3.3×10^{-3}	0.9947	18.12
Fe(II)-MMT (1)	pH 2.0	5.9×10^{-4}	0.9002	14.83	2.5×10^{-3}	0.9991	47.17
	pH 7.6	5.7×10^{-4}	0.8991	14.15	2.3×10^{-3}	0.9989	46.86
	pH 8.4	5.4×10^{-4}	0.8990	13.96	2.1×10^{-3}	0.9985	46.15
Fe(II)-MMT (2)	pH 2.0	5.8×10^{-4}	0.7598	6.96	6.8×10^{-3}	0.9999	48.38
	pH 7.6	5.6×10^{-4}	0.7591	6.89	6.5×10^{-3}	0.9997	47.86
	pH 8.4	5.2×10^{-4}	0.7487	6.23	6.2×10^{-3}	0.9995	47.21

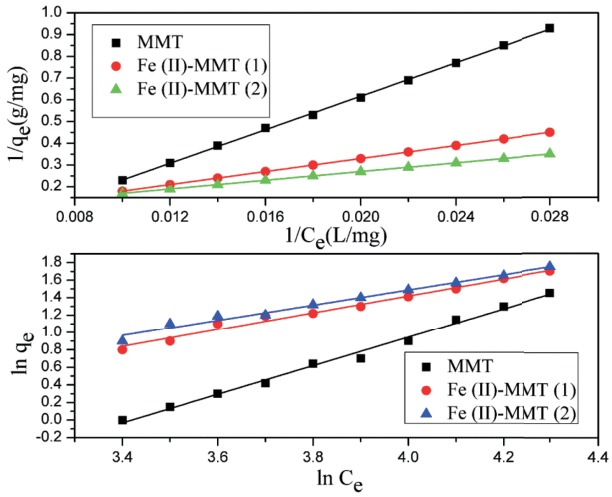

Figure 9. The Langmuir (a) and Freundlich (b) isotherm linear models for the adsorption of phosphate onto Fe(II)-MMT (1) and Fe(II)-MMT (2) (adsorption conditions: initial condition 40 mg/L, pH 2.0, and temperature 298 K).

The fitted constants of the Langmuir and Freundlich models are shown in Table 4. R^2 in the table represents the regression coefficient. The experimental data fitted the Langmuir models well ($R^2 > 0.999$), which indicates that the adsorption of phosphate on MMT, Fe(II)-MMT (1), and Fe(II)-MMT (2) was a monolayer adsorption.

Table 4. Adsorption isotherm parameters of phosphate onto three samples at different temperatures.

Samples	Temperature (K)	Langmuir isotherm			Freundlich isotherm		
		q_m (mg g^{-1})	K_L (L g^{-1})	R^2	K_F (mg g^{-1})	R^2	$1/n$
MMT	298	14.3	0.001	0.9994	0.004	0.9823	0.870
	303	15.2	0.002	0.9995	0.005	0.9825	0.875
Fe(II)-MMT (1)	310	15.5	0.002	0.9996	0.005	0.9826	0.877
	298	33.3	0.004	0.9996	0.088	0.9826	0.962
	303	35.1	0.005	0.9997	0.091	0.9827	0.966
Fe(II)-MMT (2)	310	36.4	0.006	0.9997	0.093	0.9828	0.968
	298	49.8	0.007	0.9998	0.137	0.9924	1.627
	303	50.3	0.008	0.9999	0.142	0.9925	1.633
	310	53.5	0.008	0.9999	0.145	0.9927	1.642

2.5. Thermodynamic analyses

According to the fundamental equations of thermodynamics and the Gibbs function:[37–42]

$$dG = - - SdT + Vdp \tag{5}$$

$$\Delta G = \Delta H - \Delta(TS) \tag{6}$$

The thermodynamic equations (Eqs. (7), (8), and (9)) are given by:

$$\Delta G^0 = -RT \ln K_L \tag{7}$$

$$\ln(1/C_e) = \ln K_L - \Delta H^0/(RT) \tag{8}$$

$$\Delta S^0 = (\Delta H^0 - \Delta G^0)/T \tag{9}$$

Here, K_L is the adsorption equilibrium constant; C_e (mg/L) is the equilibrium phosphate concentration in the solution; R represents the universal gas constant (8.314 J/(mol K)); and T represents the temperature in Kelvin. Table 5 summarizes the thermodynamic parameters for the three samples.

Table 5. Parameters of thermodynamics of phosphate on three samples at different temperatures.

Samples	Temperature (K)	ΔG° (kJ mol^{-1})	ΔH° (kJ mol^{-1})	ΔS° (J mol^{-1} K^{-1})
MMT	298	17.11	–6.97	–0.08
	303	16.23	–6.98	–0.09
Fe(II)-MMT (1)	310	16.14	–7.05	–0.11
	298	15.98	–7.11	–0.15
	303	15.88	–7.32	–0.17
Fe(II)-MMT (2)	310	15.78	–7.36	–0.22
	298	15.75	–7.41	–0.25
	303	15.68	–7.43	–0.27
	310	15.65	–7.52	–0.31

Because ΔG°is positive and ΔH°is negative at difference temperatures, the adsorption process is nonspontaneous and exothermic; thus, the adsorption capacity increased with temperature. This was consistent with the front end of the adsorption isotherm data.

2.6. Conclusions

Characterization of the three samples revealed that ferrous ions were adsorbed on the montmorillonite surface or in the interlayers. Phosphate adsorption of Fe(II)-MMT (1) and Fe(II)-MMT (2) was significantly higher than that of pure montmorillonite, which demonstrated that modified montmorillonite was a good adsorbent. The adsorption of phosphate onto Fe(II)-MMT (1) and Fe(II)-MMT (2) was rapid, within 40 min, and the kinetics were better described by a pseudo-second-order model. Adsorption isotherms fitted the Langmuir model better and revealed that the adsorption process was nonspontaneous and exothermic. Hence, modified montmorillonites with ferrous ions exhibited excellent removal capacity for phosphate.

3. Experimental

3.1. Chemicals and materials

The unmodified montmorillonite was obtained from Shandong SiBang Pharmaceutical Co., Ltd., and had CEC of 80 mmol/100 g. All chemicals were of analytical reagent grade and were purchased from Aladdin Reagent (China). To avoid oxidation of ferrous iron, ascorbic acid was added during its preparation and N_2-gas was used. All the pH values in the experiments were measured with a pH S-3C acidity meter.

3.2. Preparation of materials

Two different Fe(II)-montmorillonites were prepared and the ferrous iron contents were 40 mg/L and 80 mg/L. Fe(II)-MMT (1) was prepared by adding 10.0 g of MMT into 200 mL of deionized water and the pH of the suspension was adjusted to 3.5 with 1.0 M HCl. Sufficient ferrous sulfate was added to obtain a 40 mg/L Fe(II) solution, and 0.03 M ascorbic acid was dissolved. Subsequently, the suspension was oscillated in the thermostat oscillator at 25 °C for 220 min. Fe(II)-MMT (1) was obtained by centrifugation at 3500 rpm for 15 min and washed 3 times with deionized water. The resulting material was freeze-dried, passed through a 325-mesh sieve, and stored for future use.

The preparation of Fe(II)-MMT (2) was the same as Fe(II)-MMT (1) except that 80 mg/L Fe(II) solution and 0.06 M ascorbic acid were used.

3.3. Characterization of materials

The measurement of phosphate concentration followed the method proposed by Murphy and Riley.[5] The powder XRD patterns were recorded on a Bruker D8 Advance diffraction analyzer between 4°and 10°using Cu Kα radiation. FT-IR spectra of the samples were measured by KBr pressed pellet method using an IRPrestige-21 spectrophotometer. All spectra were collected at room temperature in the range of 500–4000 cm^{-1} having a resolution of 0.5 cm^{-1}. TGA and DSC were carried out on SDT-Q600 equipment with a heating rate of 10 °C/min under nitrogen. The specific surface area was measured by N_2-adsorption/desorption using a Micromeritics TriStar 3000 analyzer.

3.4. Phosphate adsorption

Adsorption experiments of phosphate onto all samples were carried out at pH 2.0, 7.6, and 8.4. For the adsorption kinetics experiment of MMT, 0.0168 g of $NaH_2PO_4 \bullet 2H_2O$ was dissolved in 250 mL of deionized water, a weighed amount of solid NaCl was added to obtain a 0.9 wt.% solution, and the pH was adjusted to 2.0, 7.6, and 8.4 by adding HCl or NaOH solutions. MMT (0.1 g) and ascorbic acid (0.03 mm) were dispersed and blended well. One milliliter of supernatant was taken out and added to a 50-mL volumetric flask, after which 1 mL of ascorbic acid solution and 2 mL of molybdate salt solutions were added, followed by dilution to 50 mL. Similarly, this procedure was applied for adsorption kinetics of Fe(II)-MMT (1) and Fe(II)-MMT (2). Adsorbed phosphate was calculated from the difference between the initial phosphate concentration and the concentration that remained. All experimental data were repeated three times and relative errors ranged within ±3%.

Acknowledgments

The work was supported by Shandong SiBang Pharmaceutical Co. Ltd. We are grateful to Beijing Purkinje General Instrument Co. Ltd. for analytical determinations and the Shandong Bureau of China Metallurgical Geology Bureau Test Center for structural analyses. We are grateful to the Shandong Province Natural Science Foundation of China (ZR2017LC005).

References

1. Noordzij, M.; Korevaar, J. C.; Boeschoten, E. W.; Dekker, F. W.; Bos, W. J.; Krediet, R. T. *Am. J. Kidney Dis.* **2005**, *46*, 925-932.
2. Isakova, T.; Gutiérrez, O. M.; Wolf, M. *Kidney Int.* **2009**, *76*, 705-716.

3. Molony, D. A.; Stephens, B. W. *Adv. Chronic. Kidney D.* **2011**, *18*, 120-131.
4. Goldberg, S; Forester, H. S.; Godfrey, C. L. *Soil. Sci.* **1996**, *60*, 425-432.
5. Murphy, J.; Riley, J. P. *Anal. Chim. Acta* **1962**, *27*, 31-36.
6. Richens, D.T. *The Chemistry of Aqua Ions*; Wiley: Chichester, UK, 1997.
7. Sinha, A.; Prasad, N. *Clin. Phys.* **2014**, *3*, 38-45.
8. Nahla, A. A.; Edress, A. M. *Nucl. Sci. Techn.* **2016**, *1*, 120-127.
9. Gulati, A.; Sridhar, V.; Bose, T.; Hari, P.; Bagga, A. *Int. Urol. Nepgrol.* **2010**, *42*, 1055-1062.
10. Gregg, S. J.; Sing, K. S. W. *J. Colloid Interf. Sci.* **1983**, *94*, 2.
11. Gros, B.; Galán, A.; Gonzálezparra, E.; Herrero, J. A.; Echave, M.; Vegter, S.; Tolley, K.; Oyagüez, I. *Health. Econ. Rev.* **2015**, *5*, 1-9.
12. Subramaniam, M. D.; Kim, I. H. *J. Anim. Sci. Biotechno.* **2016**, *1*, 41-49.
13. Freundlich, H.; Heller, W. *J. Am. Chem. Soc.* **1939**, *61*, 2228-2230.
14. Zhai, C. J.; Yang, X. W.; Sun, J.; Wang, R. *Int. Urol. Nephrol.* **2015**, *47*, 527-535.
15. Stein, D. R.; Feldman, H. A.; Gordon, C. M. *Pediatr. Nephrol.* **2012**, *27*, 1341-1350.
16. Lin, J.; Jiang, B.; Zhan, Y. *J. Environ. Manage.* **2018**, *217*, 183-195.
17. Qu, X. Y.; Chen, J. F.; He, C. Q.; Chi, F.; Johnston, S. L. *Livest. Sci.* **2018**, *210*, 15-20.
18. Levin, A.; Foley, R. N. *Am. J. Kidney Dis.* **2000**, *36*, 24-30.
19. Locatelli, F.; Marcelli, D.; Conte, F.; D'Amico, M.; Del, V. L.; Limido, A.; Malberti, F.; Spotti, D. *Nephrol. Dial. Transpl.* **2000**, *15*, 69.
20. Levin, A.; Foley, R. N. *Am. J. Kidney Dis.* **2000**, *36*, 24-30.
21. Wu, Y.; Zhou, N.; Li, W.; Gu, H.; Fan, Y.; Yuan, J. *Mat. Sci. Eng.* **2013**, *33*, 752-757.
22. Zhou, N.; Fang, S.; Xu, D.; Zhang, J.; Mo, H.; Shen, J. *Appl. Clay. Sci.* **2009**, *46*, 401-403.
23. Parida, U. K.; Nayak, A. K.; Binhani, B. K.; Nayak, P. L. *J. Biomater. Tiss. Eng.* **2011**, *2*, 414-425.
24. Chen, Y.; Bo, L.; Zhou, A.; Liang, J. *Acta Mater. Compos. Sin.* **2010**, *6*, 237-260.
25. Wang, L.; Chen, J. W.; Ren, F. M.; Wei-Bing, X. U.; Zhou, Z. F. *China J.* **2012**.
26. Wang, S. *Chinese. J. Polym. Sci.* **2014**, *6*, 675-680.
27. Langmuir, I. *J. Am. Chem. Soc.* **1915**, *37*, 208-235.
28. Borgnino, L.; Giacomelli, C. E.; Avena, M. J.; Pauli, C. *Prog. Coll. Pol. Sci. S.* **2010**, *353*, 238-244.
29. Borgnino, L.; Avena, M. J.; Pauli, C. *Colloid. Surface. A* **2009**, *341*, 46-52.
30. Freundlich, H.; Heller, W. *J. Am. Chem. Soc.* **2002**, *61*, 861-870.
31. Taddei, S.; Nami, R.; Bruno, R. M.; Quatrini, I.; Nuti, R. *Heart Fail. Rev.* **2011**, *16*, 615-620.
32. Dékány, V.; Seefeld, G.; Lagaly, G. *Clay Miner.* **2000**, *5*, 763-769.
33. Corvis, Y.; Négrier, P.; Espeau, P. *J. Pharm. Sci.* **2011**, *12*, 5235-5243.
34. Shi, X.; Rosa, R.; Lazzeri, A. *Langmuir* **2010**, *26*, 8474-8482.
35. Li, Q.; Du, Y. Z.; Yuan, H., Zhang, X. G.; Miao, J.; Cui, F. D.; Hu, F.Q. *Eur. J. Pharm. Sci.* **2010**, *41*, 3-4.
36. Tuomasjukka, S. S.; Viitanen, M. H.; Kallio, H. P. *J. Nutr. Biochem.* **2009**, *20*, 909-915.
37. Koseki, T.; Onishi, H.; Takahashi Y. *P. Soc. Photo-Opt. Ins.* **2008**, *56*, 10.
38. Li, Y.; Weng, W. *J. Mater. Sci.* **2008**, *19*, 19-25.
39. Cheng, Y.; Song, W.; Cheng J.; Zhao, B. *J. Colloid Interf. Sci.* **2007**, *307*, 447-454.

40. Lim, M. S.; Feng, K.; Chen, X.; Wu, N. Q.; Raman, A.; Nightingale, J.; Gawalt, E. S.; Korakakis, D.; Hornak, L. A.; Timperman, A. T. *Langmuir* **2007**, *23*, 5.

41. Pleite, R.; Martínez-Force, E.; Garcés, R. *J. Agr. Food. Chem.* **2006**, *54*, 9383-9388.

42. Mensink, R. P. *Lipids.* **2006**, *40*, 1201-1205.